J. Micromech. Microeng. **22** (2012) 065011 (10pp) doi:10.1088/0960-1317/22/6/065011

Focusing liquid microjets with nozzles

A J Acero[1], C Ferrera[1], J M Montanero[1,3] and A M Gañán-Calvo[2]

[1] Department of Mechanical, Energetic and Materials Engineering, University of Extremadura, Avda. de Elvas s/n, E-06006 Badajoz, Spain
[2] Department of Aerospace Engineering and Fluid Mechanics, University of Seville, Camino de los Descubrimientos s/n, E-41092 Sevilla, Spain

E-mail: jmm@unex.es

Received 19 September 2011, in final form 1 March 2012
Published 9 May 2012
Online at stacks.iop.org/JMM/22/065011

Abstract
The stability of flow focusing taking place in a converging–diverging nozzle, as well as the size of the resulting microjets, is examined experimentally in this paper. The results obtained in most aspects of the problem are similar to those of the classical plate-orifice configuration. There is, however, a notable difference between flow focusing in nozzles and in the plate-orifice configuration. In the former case, the liquid meniscus oscillates laterally (global whipping) for a significant area of the control parameter plane, a phenomenon never observed when focusing with the plate-orifice configuration. Global whipping may constitute an important drawback of flow focusing with nozzles because it reduces the robustness of the technique.

1. Introduction

The controlled production of jets at the submillimeter scale is of enormous interest in very diverse fields, such as pharmacy, biotechnology and the food and agriculture industry [1, 2]. Capillary jets are the natural precursors of the drops, bubbles, emulsions and capsules commonly used in very varied technological applications [3]. They are steadily produced in the laminar regime by injecting sufficient energy into the system to overcome the resistance offered by the surface tension and viscosity. Then, the spontaneous growth of waves on the interface gives rise ultimately to the jet pinching, producing fluid shapes whose morphology mainly depends on the jet features. Microjet production techniques must fulfil two major requirements: (i) the existence of a robust steady jetting regime, stable over a wide range of experimental conditions, and (ii) ready control of the jet features (size, shape, and internal structure) through the operational parameters.

Extensional co-flows constitute a remarkable class of techniques which satisfy the aforementioned two requirements. In this case, a force originated by a co-flowing stream stretches a fluid meniscus until a thin fluid ligament is ejected. Two driving forces can be used to expel the fluid jet: the viscous drag force exerted by an external liquid current (e.g., the viscous withdrawal [4, 5] and the parallel co-flow configurations [6]), and the suction force caused by the pressure drop induced by a co-flowing fluid stream (flow focusing [7]). The flow-focusing technique [7] working in the so-called jetting mode uses the pressure gradient induced by an outer gas stream to 'focus' a steady liquid meniscus from whose tip a microjet is emitted. Both the liquid microjet and the co-flowing gas stream cross a discharge orifice whose diameter is much larger than that of the microjet. Steady jetting is obtained with flow focusing for a wide range of operational conditions. The jet size is precisely controlled by selecting appropriately the liquid flow rate and the applied pressure drop. This technique is very attractive because it uses purely hydrodynamic means to produce monodisperse collections of micrometer drops at a continuous high rate [7]. When the outer axisymmetric gas stream is replaced with a co-flowing liquid, flow focusing gives rise to emulsions and microcapsules with a narrowly controlled size and morphology [8]. Stable high-speed drawing of fibers can also be obtained by focusing highly viscous jets with this co-flowing arrangement [9].

In the standard flow-focusing configuration, sometimes referred to as 'axisymmetric flow focusing', a feeding capillary is located in front of a plate with a circular orifice of diameter similar to that of the capillary. The liquid is injected through the capillary, while the gas stream is originated in a surrounding pressurized chamber. This configuration has been successfully adapted to the 2D topology to produce emulsions [10] and bubbles [11] down to the micrometer scale. The steady jetting stability can be regarded as the sum of the stability of the

[3] Author to whom any correspondence should be address.

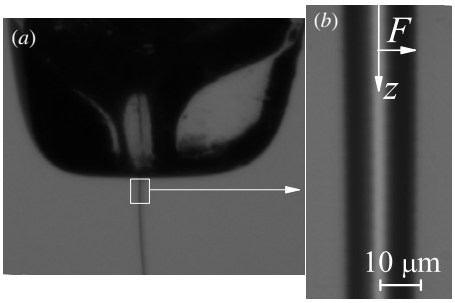

Figure 1. (*a*) Microjet of 35 cSt silicone oil moving with a flow rate $Q = 5$ ml h^{-1} inside a co-flowing air stream driven by a pressure drop $\Delta p = 105$ mbar. Both the liquid and gas streams were produced with the glass micro-nozzle considered in this work. (*b*) Zoom lens image of a 500 cSt silicone oil microjet next to the discharge orifice.

tapering liquid meniscus and of the emitted jet. Thus, obtaining a steady meniscus has to be considered as a prerequisite to achieving steady jetting, while the absence of absolute instability in the jet is the additional necessary condition. Following this strategy, the steady jetting stability has been successfully analyzed over a wide range of experimental conditions [12–15]. The injected flow rate has been found to be the key parameter which determines the meniscus stability for sufficiently large applied pressures [15]. The meniscus stability can also be limited by the energy sink in the meniscus tip due to surface tension [13]. For low-viscosity liquids and small applied pressure drops, the jet absolute instability [16, 17] plays an essential role because it allows growing perturbations to travel upstream and pinch the free surface at the emission point [12–14]. The shape and size of microjets produced by the standard flow-focusing configuration have recently been examined over a wide range of experimental conditions [18]. By appropriately scaling the variables of the problem, the microjet shape was accurately described by a universal solution [19, 20] which covers from the very viscous to the almost inviscid regimes.

The flame-shaped glass micro-nozzle has recently been proposed as an alternative device for flow focusing [21]. When a flame is applied to the tip of a clean-cut millimeter glass tube, the glass melts and flows, driven by the surface tension and viscosity forces, which narrows the inner duct formed in the tube. If the heat source is swiftly withdrawn before the glass inner free surface pinches, the glass solidifies into a variety of hour-glass shapes depending on the flame's intensity, focus and location. Almost roughness-free, converging–diverging nozzles are obtained as a result of this process [22]. The nebulizer is built by introducing concentrically a feeding capillary inside the converging–diverging nozzle. To obtain the flow-focusing effect, the liquid is injected through the capillary while a gas stream crosses the nozzle driven by the action of an applied pressure drop. As in the standard plate-orifice configuration, the gas stream suctions the liquid meniscus attached to the capillary from whose tip a microjet tapers (figure 1). The main advantages offered by these nozzles over the classical plate-orifice configuration are as follows: (i) they are smooth even at the micrometer scale, (ii) one can readily obtain nozzles with neck diameters in the range of a few tens of microns, (iii) they demand gas flow rates (energy) significantly smaller than those required by the plate-orifice configuration and (iv) they are transparent. Because of these advantages, glass micro-nozzle has recently been used to flow-focusing hydrated streams of nanocrystals in a novel x-ray crystallography method [23]. However, there can be significant differences between the gas flow patterns in the plate-orifice configuration and the converging–diverging nozzle. Specifically, the axial momentum of the gas stream close to the feeding capillary end is significantly larger in the nozzle than in the plate-orifice configuration, which may alter the meniscus stability. In addition, the nozzle shape might modify considerably the momentum transfer between the gas stream and the liquid jet, which would result in different jet sizes at the discharge orifice.

In this paper, we analyze experimentally the flow-focusing phenomenon in a micrometer nozzle by examining both the stability of the steady jetting regime and the size of the emitted jets. Since the instability modes of elongated liquid shapes differ from those of short ones, one may expect the shorter liquid menisci formed in the plate-orifice configuration to behave differently from their elongated counterparts in the configuration studied here. In addition, the much higher axial velocity of the gas sheath in the later configuration must necessarily affect the meniscus dynamics. A type of meniscus instability, not present in the classical plate-orifice configuration [12, 14, 15], is observed in the present experiments. This instability makes the liquid meniscus oscillate laterally. In some cases, the oscillation is so violent that the meniscus hits the nozzle's inner walls and the liquid ejection is interrupted. Moreover, the jet size at the discharge orifice is significantly smaller than that measured with the standard configuration owing to the action of viscous stresses on the free surface inside the nozzle.

The paper is organized as follows. The flow-focusing phenomenon in a nozzle is briefly described in section 2. The experimental setup and procedure are described in section 3. Section 4 presents the stability results for the liquid meniscus (section 4.1) and the emitted jet (section 4.2). The jet size is analyzed in section 5. Finally, the paper closes with some conclusions in section 6.

2. Nozzles versus the plate-orifice configuration

In flow focusing, a liquid of density ρ and viscosity μ is injected at a constant flow rate Q through a feeding capillary of radius R_1. The liquid forms a meniscus attached to the capillary end held by the surface tension σ. The liquid meniscus is stretched by the action of a gas stream driven by the difference Δp between the pressure of the gas reservoir and that of the environment. A thin liquid jet tapers from the meniscus tip which co-flows with the gas current. In the standard plate-orifice configuration, both the liquid jet and the external gas stream cross an orifice of diameter D in a plate located at a distance H in front of the capillary. In flow focusing with nozzles, the fluids cross an axisymmetric converging–diverging nozzle with diameters D_n and D_{out} at the neck and outlet sections, respectively. In this case, H is the distance

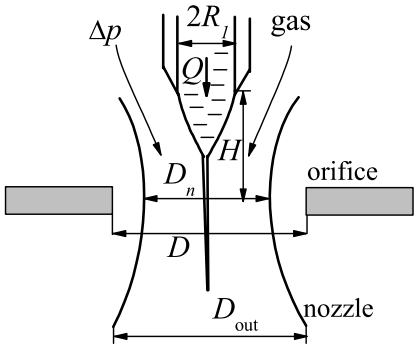

Figure 2. The plate-orifice and nozzle configurations.

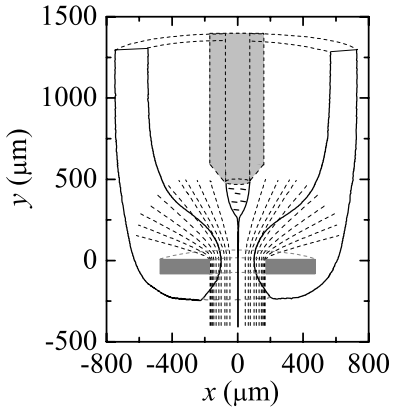

Figure 3. The nozzle used in our experiments and the equivalent plate-orifice configuration. The figure shows the nozzle contour obtained by processing digital images of the nozzle immersed in a glycerine bath to eliminate the optical distortion [22]. The dashed lines in front of the nozzle neck are the streamlines (1) of the potential flow crossing an orifice of diameter $D = D_{eq} = 346$ μm. The dashed lines beyond the orifice depict the streamlines in the region. The capillary contour and the liquid free surface are also depicted in the figure.

between the capillary end and the nozzle neck. Figure 2 depicts both the plate-orifice and the nozzle configurations.

The same liquid injection system is used in both the plate-orifice and nozzle configurations. Therefore, the differences between them are due to the gas flow. The gas flow pattern in the plate-orifice configuration is essentially determined by the orifice diameter D. Because the Reynolds number $Re_g = (\rho_g \Delta p)^{1/2} D_n/\mu_g$ (ρ_g and μ_g are the gas density and viscosity, respectively) takes large values in the gas domain, the streamlines in front of the discharge orifice approximately coincide with those of the potential flow approximation. The streamlines characterizing the potential flow across a zero-width orifice are given by the parametric equations [24]

$$x = D(1+\xi^2)^{1/2}(1-\eta^2)^{1/2}, \quad y = D\xi\eta. \tag{1}$$

Here, x and y are the horizontal and upward vertical axes, respectively, with the origin at the orifice center (figure 3). The streamlines in front of the orifice are obtained by varying the parameter ξ within the interval $0 \leqslant \xi \leqslant \infty$ while keeping η ($0 \leqslant \eta \leqslant 1$) constant. In flow focusing with nozzles, the contour of the nozzle converging part practically coincides with a stream tube due to the negligible thickness of the gas boundary layer in that part of the nozzle. One can define the

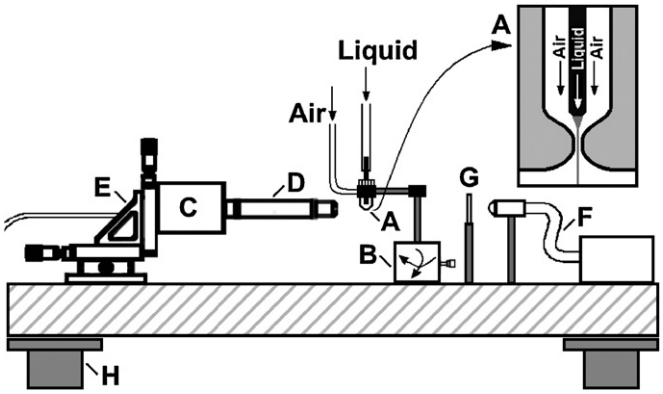

Figure 4. Experimental setup: nozzle (A), dual-axis goniometer (B), video camera (C), optical lens (D), triaxial translation stage (E), optical fiber connected to a stroboscopic light source (F), frosted diffuser (G) and optical table (H). The scheme of the flow-focusing device is shown magnified at the top right.

equivalent orifice diameter D_{eq} of a nozzle as the D value in (1) for which a streamline approximately fits the contour of the nozzle converging part. Figure 3 illustrates this idea. The solid line corresponds to the contour of the nozzles used in the experiments, while the dashed lines in front of the orifice are streamlines (1) with $D = D_{eq} = 346$ μm. The dashed lines beyond the orifice depict the streamlines in that region, which cannot be obtained from the inviscid approximation. The capillary contour and the liquid free surface are also represented in the figure. Because D_{eq} is much greater than D_n, the gas (energy) consumed by the nozzle is much less than that used by the equivalent plate-orifice configuration.

3. The experimental method

Figure 4 shows the experimental setup used in the present study. The nebulizer (A) consisted of a capillary tube of inner radius $R_1 = 77$ μm located inside a glass converging–diverging nozzle with characteristic diameters $D_n = 194$ μm and $D_{out} = 400$ μm at the neck and outlet sections, respectively. We selected this nozzle because it significantly deviates from the plate-orifice configuration in both converging and diverging sections. A liquid was injected at a constant flow rate Q with an infusion pump through the capillary tube, whose end was sharpened to force the triple contact line to attach to its inner diameter. Air was injected through a pneumatic circuit by applying a constant pressure drop Δp. The nozzle was oriented with a dual-axis goniometer (B). Digital images of 1280 × 960 pixels were acquired at 30 frames per second using a CCD camera (AVT Stringay F-1125B) (C) equipped with optical lenses (an Optem ZOOM 70XL set of lenses with variable magnification from 0.75× to 5.25×) (D) providing a frame covering an area of about 96.78 × 72.58 μm^2. The magnification obtained was approximately 76 nm/pixel. The camera could be displaced both horizontally and vertically using a triaxial translation stage (E) to focus either the liquid meniscus or the emitted microjet. The fluid configuration was illuminated from the back side of the experimental apparatus by cool white light

Table 1. Properties of the focused liquids at 20 °C.

Liquid	ρ (kgm^{-3})	σ (Nm^{-1})	μ (Pa s)
500 cSt silicone oil	970	0.020	0.48
100 cSt silicone oil	961	0.021	0.096
35 cSt silicone oil	957	0.020	0.033
5 cSt silicone oil	917	0.019	0.0046
Water	998	0.072	0.0010

provided by an optical fiber (F). The optical fiber was connected to a stroboscopic light source to reduce the image exposure time to about 3 μs. A frosted diffuser (G) was positioned between the optical fiber and the microjet to provide uniform lighting. All these elements were mounted on an optical table (H).

Before conducting the experiments, the inner nozzle contour was measured with the method described in [22]. For this purpose, the nozzle was put in a liquid bath with almost the same refractive index as that of the nozzle to practically eliminate any optical distortion. A digital image of the nozzle was acquired with a microscope using back-light illumination to obtain a silhouette effect. The image was processed to locate the contours of the nozzle with a high resolution. Figure 3 shows the contours detected. The surface tension of the working liquids was measured with the theoretical image fitting analysis method [25]. The viscosity and density values were taken from the manufacturer's specifications. The liquids listed in table 1 were focused with air at 20 ± 2 °C.

The stability of the liquid meniscus was examined for different values of the capillary-to-neck distance H. To select the value of H, the capillary was displaced inside the nozzle. During this operation, the nozzle was immersed in a liquid bath with almost the same refractive index as that of the nozzle, and rotated in front of the camera to ensure correct alignment. Once the capillary-to-neck distance was fixed, an experimental run was conducted according to the following steps. We first set the pressure drop Δp in the gas stream. Then, a liquid flow rate Q was injected through the capillary. After a short transient regime, a liquid meniscus was formed attached to the capillary edge. Images of either the liquid meniscus or the emitted jet were acquired and recorded. The liquid flow rate Q was reduced in steps of 0.1 ml h^{-1} until the different regimes were observed. The images of the emitted jets were processed to detect the free surface position. The jet radius R_j was calculated by fitting the following expression to the experimental contour (figure 1(b)):

$$F(z) = R_j + a\,\mathrm{e}^{\gamma z}\cos(kz + \phi), \tag{2}$$

which corresponds to a surface wave growing on a jet of radius R_j with spatial growth factor γ and wavelength k. Figure 1(b) shows the images of the 500 cSt silicone oil microjet. In this case, viscous stresses prevented surface waves from growing, and thus an almost cylindrical jet was observed next to the discharge orifice.

4. Stability

4.1. Stability of the liquid meniscus

The most relevant result of this paper is the appearance of a 'global whipping' regime in a significant region of the parameter plane. In this regime, the liquid meniscus oscillates laterally while continuously emitting a microjet, a phenomenon not previously observed with the plate-orifice configuration [12, 14, 15]. In fact, whipping oscillations are believed to be always convected downstream when producing capillary jets not only with flow focusing but also with other means. The convection of whipping oscillations downstream has been observed in, for instance, the electrospray of low electrical conductivity liquids in the cone-jet mode [26], the electrospinning of polymer jets [27], and the atomization of low-viscosity liquid jets in a coaxial gas stream at moderately high Weber numbers [28]. In all these cases, the liquid stream sweeps away growing surface waves, preserving a stable liquid source at the emission point. It is worth noting that lateral perturbations may propagate upstream over the jet when focusing very viscous liquids with the standard plate-orifice configuration. In this case, self-sustained sinuous oscillations can be observed next to but beyond the exit orifice. Even in this case, the meniscus remained stable because the perturbations cannot overcome the plate orifice. Global whipping is essentially different from the behaviors mentioned above because the lateral oscillations spread over the entire liquid domain in this case. It is similar to the sinuous oscillations of two-dimensional jets and wakes with moderately high Reynolds numbers recently obtained from a global linear stability analysis [29].

Figure 5 (left and center) shows images of a glycerol jet at the exit orifice of a plate-orifice flow-focusing device. The left image corresponds to the convection of whipping oscillations downstream, preserving the tapering meniscus stable. The central photograph is the superposition of three images of a jet of about 42 μm in diameter, all of them acquired with a high-speed video camera under the same conditions but with different exposure times to show the jet behavior in this regime. The image with the longest exposure time shows how the liquid fans out due to the violent oscillations. The two jet's extreme positions form an angle of about 24.6°. There are also two images acquired with an exposure time of 10 μs to show the instantaneous jet position. In the experiment shown in figure 5 (center), lateral perturbations propagated upstream leading to violent bending oscillations of the jet at the exit orifice. However, the meniscus remained stable. Figure 5 (right) shows two images of a 5 cSt silicone oil meniscus laterally oscillating inside the glass nozzle just when global whipping appears. The amplitude of the free surface oscillation increases as the distance from the feeding capillary increases. The amplitude at the bottom of the image is about 25 μm (about one third of the nozzle neck radius). The transition from the stable regime to this global whipping behavior is sufficiently sharp to be detected without applying image processing techniques.

Figure 6 shows the stability regimes found for $H = 440$ μm and different liquids. Similar results were obtained for other capillary-to-orifice distances. As can be observed, the

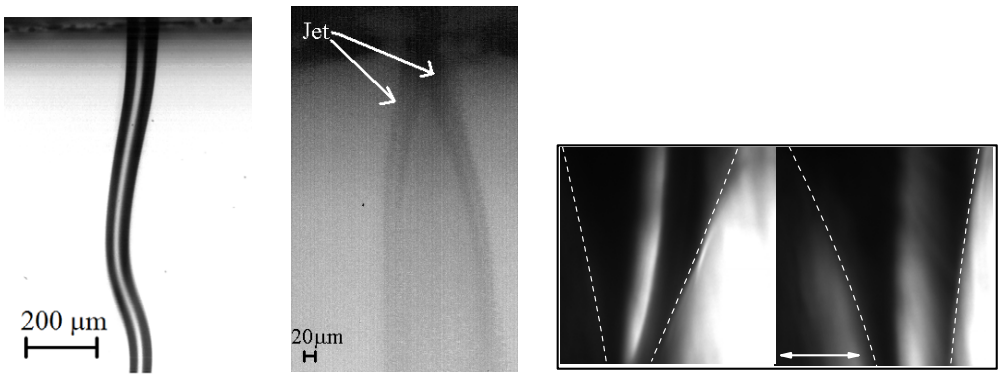

Figure 5. Left: convection downstream of whipping oscillations over a glycerol jet produced by a plate-orifice flow-focusing device. Center: superposition of three images of a glycerol jet at the exit orifice of a plate-orifice device. Two of them acquired with an exposure time of 10 μs to show the instantaneous jet position, and the third with an exposure time of 5 ms to show how the liquid fans out due to the violent oscillations. Right: images of a 5 cSt solicone oil meniscus oscillating inside the glass nozzle when global whipping appears.

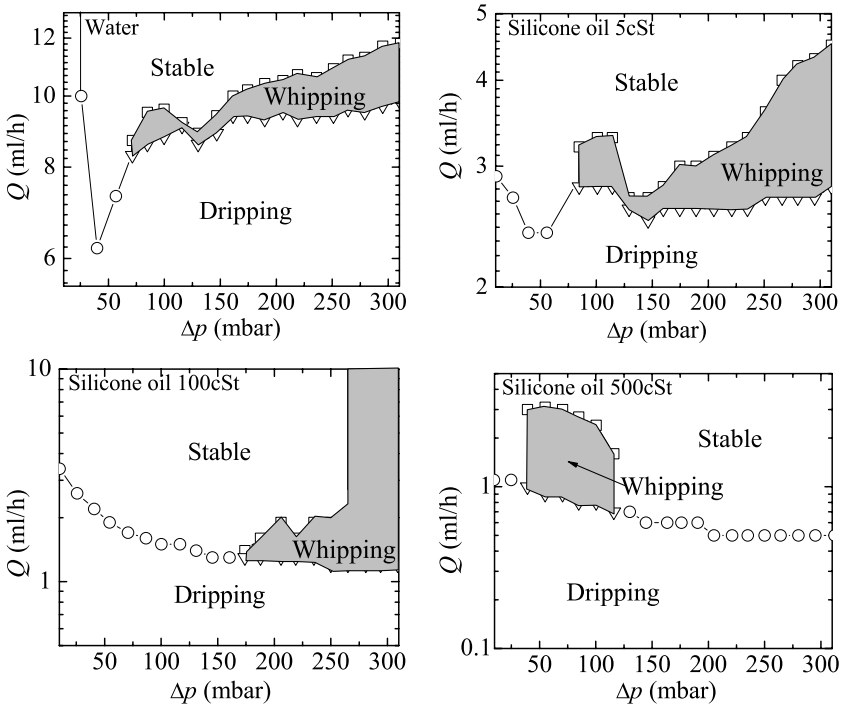

Figure 6. Stability regions of the liquid meniscus for $H = 440$ μm.

shape and size of the global whipping region in the $(Q, \Delta p)$ plane depends on the liquid properties. It generally appears for flow rates close to the dripping transition, and sufficiently large pressure drops. However, global whipping was not observed for large pressure drops in the 500 cSt silicone oil case. This complex dependence of the whipping instability with respect to the parameters of the problem reflects the intricate nature of the phenomenon. Unfortunately, we could not inject higher viscosity liquids due to the very small radius of the feeding capillary. In these cases, the transitory regimes (start and stop) and the associated highly unsteady behavior of the elongated liquid meniscus caused irreversible clogging (the device needed cleaning and flushing).

We verified that the lateral meniscus oscillations were not caused by a possible misalignment of the feeding capillary and the glass nozzle. For this purpose, we moved the capillary laterally a short distance along several directions and verified that the results did not vary significantly. Global whipping is caused by the growth of the lateral $m \geqslant 1$ modes which lead to *self-sustained* oscillations of the liquid meniscus (as the vortex shedding process taking place in the wake of a blunt body [30], or the sinuous oscillations in two-dimensional co-flows [29]). The evolution of lateral perturbations is the result of the competition between the destabilizing aerodynamic pressure $\rho_g(V_g - V_l)^2$ (V_g and V_l are typical values of the velocities parallel to the free surface in the gas and liquid domains, respectively) associated with the velocity slip $V_g - V_l$ and the restoring capillary stress σ/R_j due to the surface tension [28, 31]. The lateral oscillations of the liquid meniscus may originate either in the liquid meniscus, where the stabilizing capillary stress is smaller, or in the emitted jet, where the destabilizing aerodynamic pressure is larger. In this latter case,

the perturbations propagate both downstream and upstream (absolute instability [17]), causing the liquid to fan out [32]. A similar phenomenon has been observed in coaxial injectors where the stabilizing effect of the surface tension is negligible [33], as in two-dimensional jets and wakes with low and intermediate surface tensions [34]. Elucidating the origin of the global whipping would require the use of high-speed visualization inside the nozzle, which constitutes a very difficult problem technically. A natural question is why this phenomenon has not been observed when focusing with the plate-orifice device, in spite of the numerous experiments performed to examine the liquid meniscus behavior with this configuration [12, 14, 15]. In this case, the gas flow is more radial around the liquid meniscus, and hence the velocity slip takes smaller values in this region, thus inhibiting the growth of lateral oscillations. The orifice acts as a barrier for lateral waves, preventing their propagation toward the feeding capillary.

The liquid meniscus drips for flow rates smaller than a threshold value $Q_{\min}$ which depends on the applied pressure drop Δp. As occurs with the plate-orifice configuration, the minimum flow rate $Q_{\min}$ below which the liquid meniscus becomes unstable is practically independent of the applied pressure drop for sufficiently large values of this quantity. Because of its relevance in most flow-focusing applications, here we shall center on this case. We measured $Q_{\min}$ for $\Delta p = 250$ mbar and different values of the capillary-to-neck distance H. For each liquid considered, there was an optimum value of H for which the critical flow rate $Q_{\min}$ reached its limiting value; $Q_{\lim}$. $Q_{\lim}$ is probably the key parameter in flow focusing because it delimits the parameter region where global stability cannot be attained. As shown in [15], the relationship between $Q_{\lim}$ and the rest of the relevant variables can be written as $Q_{\lim}/Q_v = G(Q_{\lim}/Q_D)$, where $Q_D \equiv D_{\text{eq}}\mu/\rho$ and $Q_v \equiv R_1^2\sigma/\mu$ are the characteristic flow rates for which the meniscus instability is expected to occur in the low- and high-viscosity regimes, respectively. In the first case, instability is caused by the interaction between the recirculation cell appearing in the liquid meniscus and the inner wall of the feeding capillary [13]. In the high-viscosity regime, the liquid meniscus becomes unstable because the surface tension stress overcomes the driving pressure drop Δp, thus preventing a steady meniscus from being formed [15].

Figure 7 shows $Q_{\lim}/Q_D$ versus $Q_{\lim}/Q_v$ for the liquids listed in table 1. The gray symbols are the limiting flow rates obtained in [15] with the standard plate-orifice configuration. There is remarkable agreement between the results obtained with the two configurations, which shows the high degree of generality of the conclusions drawn from the analysis in [15]. The limiting flow rate $Q_{\lim}$ for 5 cSt silicone oil is slightly larger than the general trend shown by the dashed line. This is because in this case, global whipping prevented us from reaching the optimum capillary-to-neck distance H. For relatively small values of this parameter, the lateral oscillations of the liquid meniscus made it collide with the nozzle which halted the liquid ejection.

Both low- and high-viscosity regimes can be easily identified in figure 7. The low-viscosity regime corresponds to

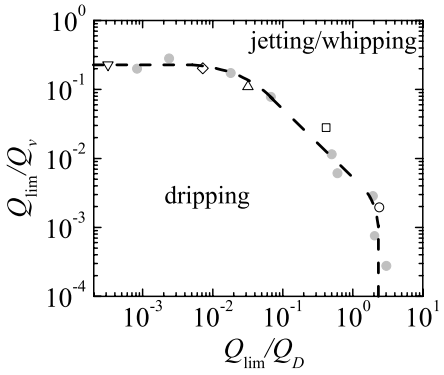

Figure 7. $Q_{\lim}/Q_D$ versus $Q_{\lim}/Q_v$ for the liquids listed in table 1. The circle, square, up-triangle, diamond, and down-triangle correspond to water, 5 cSt silicone oil, 35 cSt silicone oil, 100 cSt silicone oil, and 500 cSt silicone oil, respectively. The gray symbols are the limiting flow rates obtained in [15] with the standard plate-orifice configuration. The dashed line is to guide the eye.

the right vertical segment of the stability curve, for which Q_D/Q_v (which is of the order of the Ohnesorge number $\text{Oh} = \mu^2/(\rho\sigma R_1)$) takes very small values. In this regime, $Q_{\lim} \sim Q_D$, as predicted in the scaling analysis presented in [15]. The left horizontal part of the stability curve corresponds to the regime dominated by viscosity ($\text{Oh} \gg 1$). There is a smooth transition between the two limiting behaviors. The line drawn on the stability map approximately delimits the dripping region.

4.2. Stability of the emitted jet

The stability of the liquid source (meniscus) is a prerequisite for obtaining stable jets. Local instabilities appearing in the emitted jets can further narrow the steady jetting region. For this reason, the stability analysis presented in the previous section must be completed by observing the behavior of the tapering jet at the nozzle discharge orifice. Figure 8 shows the results obtained for $H = 440$ μm plotted on the plane defined by the Reynolds $Re = \rho VR/\mu$ and Weber $We = \rho V^2 R/\sigma$ numbers. Here, R is the jet radius given by the first-order approximation [7]

$$R = \left(\frac{\rho Q^2}{2\pi^2 \Delta p}\right)^{1/4}, \tag{3}$$

where one neglects the loss of kinetic energy owing to viscous dissipation and surface tension. In addition, $V = Q/(\pi R^2)$ is the velocity averaged over the jet cross-section. The white, black and gray symbols correspond to the jetting, dripping and whipping regimes, respectively. In this case, the (local) whipping regime corresponds to the lateral oscillation of the emitted jet, independently of what occurs to the tapering liquid meniscus. As mentioned above, local (convective) whipping is a phenomenon commonly observed in capillary jets [26–28].

One can distinguish two types of jetting/whipping to dripping transitions: one occurring for large Δp at a practically constant flow rate $Q = Q_{\min}$, and the other for small Δp and different values of the injected flow rate Q. The corresponding stability limits form an elbow for each liquid in the (We, Re) plane. The transition for large Δp corresponds to the stability

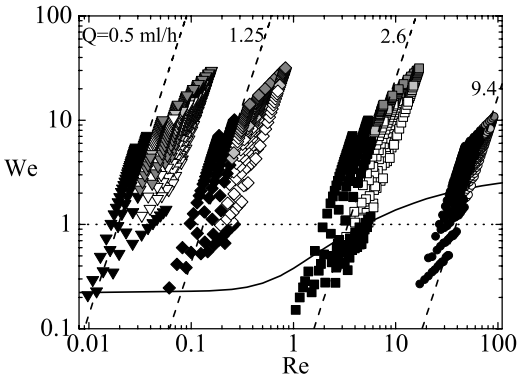

Figure 8. Stability regions of the emitted jet in the (*We*, *Re*) plane for $H = 440\ \mu$m. The circles, squares, diamonds and triangles correspond to water, 5 cSt silicone oil, 100 cSt silicone oil and 500 cSt silicone oil, respectively. The white, black and gray symbols correspond to the jetting, dripping and whipping regimes, respectively. The light gray symbols indicate the transitional values from jetting to whipping. The solid line is Leib and Goldstein's prediction for the convective/absolute instability transition in a capillary jet. The dashed lines are the curves $Q = \text{const}$. The labels indicate the corresponding flow rates as obtained from the jetting/whipping to dripping transition for $\Delta p = 250$ mbar in figure 6. The dotted line is the boundary We = 1.

loss of the liquid meniscus described in the previous section. This transition is indicated by the dashed lines $Q = Q_{\min}$, with $Q_{\min}$ being the critical flow rate obtained from figure 6 for $\Delta p = 250$ mbar. The nature of the dripping transition for small Δp is different and depends on the liquid viscosity. For low-viscosity liquids (water), the steady jetting regime becomes unstable due to the convective/absolute instability transition in the emitted jet [16, 17]. The experimental data agreed reasonably well with the prediction obtained from the linear stability analysis of the uniform basic flow (solid line) [35]. The fact that the theoretical prediction slightly overestimates the transitional Weber number is due to the simplicity of the basic flow considered [13, 12]. Owing to the co-flowing gas stream, the jet's free surface moves with a velocity slightly greater than that of the bulk, which naturally favors the jet's sweeping growing surface waves downstream, displacing the onset of dripping to lower flow rates (Weber numbers). For very viscous liquids (100 and 500 cSt silicone oils), the dripping transition can be attributed to the lack of kinetic energy to overcome a surface tension at the meniscus tip [13]. Surface tension consumes a significant amount of the (small) applied energy when the jet is emitted with small flow rates. This loss of kinetic energy halts the emission. Then, the meniscus tip becomes blunt and the free surface energy sink disappears. The meniscus inflates until a portion of its tip becomes drawn into the orifice and ejected as an unsteady spitting. In this situation, the flow becomes unstable because the surface tension energy sink appears and disappears intermittently with the liquid emissions. As occurs in the plate-orifice configuration, this mechanism is responsible for the stability limit We = 1 (dotted line), which corresponds to equal kinetic and surface tension energies. As observed in figure 8, this stability limit prevails over the jet absolute instability in highly viscous jet, where surface waves are damped.

As mentioned in the previous section, the lateral oscillation of the liquid meniscus (global whipping) is a new phenomenon not previously observed in the numerous experiments conducted with the plate-orifice configuration [12–14]. In the plate-orifice case, the whipping phenomenon is confined to the jet region, i.e. beyond the discharge orifice. A natural question is whether there can be local whipping when focusing with nozzles, i.e. experimental realizations where the emitted jet oscillates laterally while the liquid meniscus remains steady. Figure 9 shows the global and local whipping regions in the control parameter plane (Δp, Q). Naturally, the local whipping regions contain those of global whipping because the meniscus oscillations make the jet oscillate too. However, there are considerable regions of the parameter plane where the jet oscillates and the meniscus remains stable. In this case, the lateral perturbations cannot travel upstream because they are blocked somewhere inside the nozzle. For instance, the results for 500 cSt silicone oil show that for sufficiently large values of the applied pressure drop, the meniscus remains stable while the jet oscillates laterally owing to the larger values reached by the destabilizing aerodynamic pressure in that region. This is the behavior observed in the classical plate-orifice configuration.

5. The jet size

The stability of the jetting regime was examined in the previous section. Here, we analyze the size of the jets emitted in that regime. Figure 10 shows the jet radius R_j measured at the nozzle exit for $H = 440\ \mu$m. As expected, the general trend indicates that the jet radius increases as viscosity increases due to the energy dissipated by viscous stresses. The results are compared with the theoretical prediction (3) obtained by equating the energy injected into the liquid through the pressure drop and its kinetic energy [7, 13]. Interestingly, one obtains jets significantly thinner (faster) than those predicted by the ideal approximation (3), in spite of the fact that both viscous and surface tension effects are neglected in that approximation. This is because of the action of the drag force exerted by the high-speed gas stream inside the nozzle. This force collaborates with the suction effect of the pressure drop on propelling the microjet. This contribution becomes more notable as the radius (volume per unit surface) decreases.

As mentioned above, the jets produced by flow focusing in nozzles are shaped by both the pressure drop in the axial direction in front of the nozzle neck and the drag force throughout the nozzle caused by the difference between the gas stream and jet velocities. It is well known that the jet shape can be satisfactorily described by the momentum equation obtained from the slenderness approximation [1]. Analogous to the plate-orifice case [18], one assumes that the total momentum injected into the jet by the suction and drag forces is constant along the length of the nozzle and proportional to the ratio of the pressure drop to a transversal characteristic length (e.g., the nozzle neck diameter D_n). One also neglects the role played by the surface tension except for very low flow

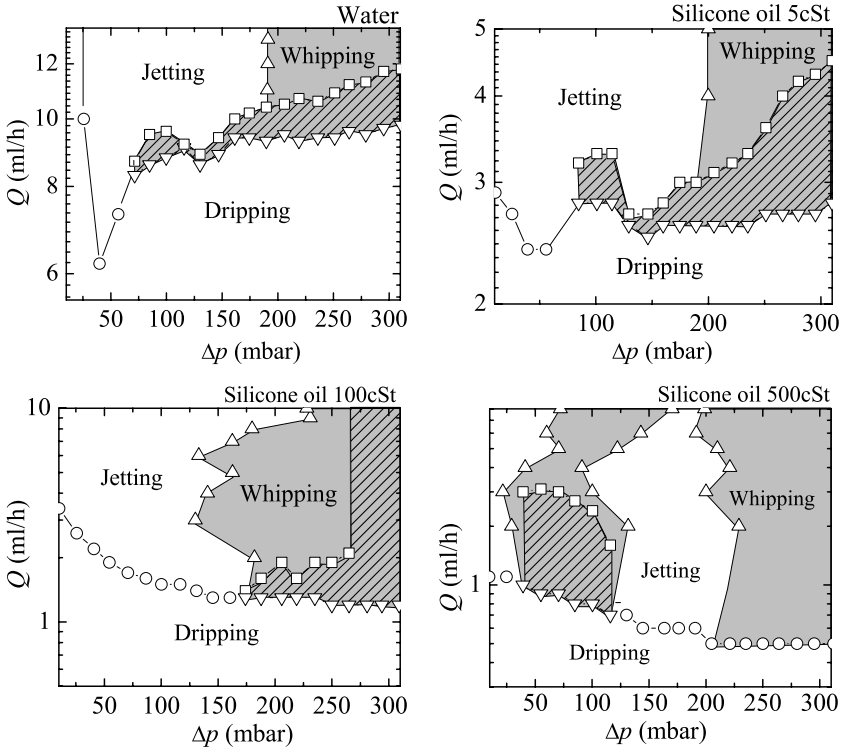

Figure 9. Stability regions for $H = 440\ \mu$m. The gray and ruled regions correspond to the lateral oscillations of the jet and liquid meniscus, respectively.

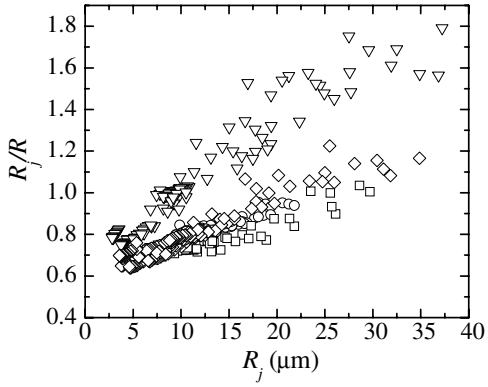

Figure 10. Jet radius R_j measured at the nozzle exit for different values of the applied pressure Δp and the liquid flow rate Q. The circles, squares, diamonds and triangles correspond to the results obtained for $H = 440\ \mu$m with water, 5 cSt silicone oil, 100 cSt silicone oil and 500 cSt silicone oil, respectively.

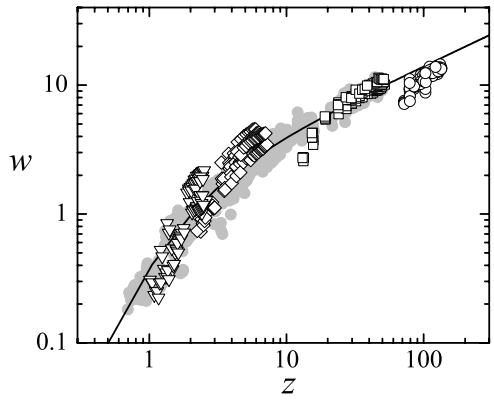

Figure 11. Scaled axial velocity w averaged over the jet cross-section as a function of the scaled axial coordinate z. The solid line is the universal solution (5). The white circles, squares, diamonds and triangles correspond to the experimental results obtained for $H = 440\ \mu$m with water, 5 cSt silicone oil, 100 cSt silicone oil and 500 cSt silicone oil, respectively. The gray symbols are the results obtained in [18] with the standard plate-orifice configuration.

rates, close to the stability limits [18]. Under these conditions, the momentum equation reduces to

$$w\frac{\mathrm{d}w}{\mathrm{d}z} - w\frac{\mathrm{d}}{\mathrm{d}z}\left(\frac{1}{w}\frac{\mathrm{d}w}{\mathrm{d}z}\right) = 1\ , \tag{4}$$

where the axial coordinate z and mean velocity w are scaled with the characteristic length $L_0 \equiv 3^{2/3}(\mu^2 D_n/\rho\Delta p)^{1/3}$ and velocity $v_0 \equiv (L_0\Delta p/\rho D_n)^{1/2}$, respectively. The physically meaningful solution of (4) satisfying the boundary conditions $w(0) = 0$ and $w \to \infty$ as $z \to \infty$ is [19, 20]

$$w = \frac{2^{-1/3}\mathrm{Ai}^2(\xi)}{\mathrm{Ai}'^2(\xi) - \xi\,\mathrm{Ai}^2(\xi)}, \quad \xi = 2^{-1/3}(z-k), \tag{5}$$

where Ai and Ai′ are the Airy function and its derivative, respectively, and $k = 2.94583\ldots$ is the first zero of $\mathrm{Ai}(-k/2^{1/3})$ for $k > 0$. The axial velocity distribution $w(z)$ given by (5) is universal, i.e. it does not depend on any variables or fitting parameters. In order to establish a comparison between that universal solution and our results, we impose the condition that (5) and the corresponding experimental value $Q/(\pi R_j^2)v_0^{-1}$ coincide at the capillary end position.

Figure 11 shows the scaled axial velocity w as a function of the scaled axial coordinate z measured for $H = 440\ \mu$m. The

solid line is the universal solution (5), while the gray symbols are the results obtained in [18] with the standard plate-orifice configuration. As in the plate-orifice case, the experimental results lie approximately on the curve (5). The scatter of the results can be attributed to the influence of the Weber number and the experimental uncertainty. The discrepancy with respect to (5) is mainly caused by the lack of uniformity of the driving force along the length of the nozzle, which may become relevant for $H/D_n \gtrsim 1$ ($H/D_n = 2.3$ in our case).

6. Conclusions

The stability and size of microjets produced by flow focusing with a converging–diverging nozzle were examined experimentally. Many results were similar to those previously obtained for the classical plate-orifice configuration. The liquid meniscus drips for flow rates below a critical value $Q_{\min}$, which becomes independent of the applied pressure drop Δp for large values of this parameter. There is an optimum position of the feeding capillary in the nozzle for which $Q_{\min}$ reaches its limiting value $Q_{\lim}$. The results for $Q_{\lim}$ practically coincide with those obtained for the plate-orifice configuration when this quantity is appropriately scaled using the equivalent plate-orifice diameter D_{eq}. This parameter is the diameter of the orifice which produces a gas flow pattern similar to that obtained with the nozzle. The analysis of the jet stability reveals the existence of three instability mechanisms: the aforementioned meniscus instability, the convective/absolute instability transition in the jet and the local instability at the meniscus tip due to surface tension effects. Finally, the jet size at the nozzle discharge orifice can be satisfactorily described by the universal Clarke solution (5).

There is an important difference between flow focusing in nozzles and in the plate-orifice configuration. In the former case, and at least for the nozzle considered in this work, there is a significant region of the parameter plane (Q, Δp) where the liquid meniscus oscillates laterally (global whipping). This phenomenon may constitute an important drawback of nozzles relative to the plate-orifice configuration because it reduces the technique's robustness, one of the main advantages of flow focusing over other jet production methods such as electrospray. In fact, we verified that the oscillations make the liquid meniscus hit the nozzle inner contour for small capillary-to-neck distances H, thus interrupting the liquid emission. It must be noted that the optimum liquid flow rates are obtained for relatively small values of that distance, and thus global whipping may significantly reduce the device's performance. The use of nozzles with higher converging rates may eliminate global whipping or reduce its effects (the analysis of this possibility is beyond the scope of the present study). On the other hand, using nozzles instead of the plate-orifice configuration offers some important advantages (smoothness, transparency, energetic efficiency, ...) when working within the 'safe' parameter region where global whipping is not expected. The present analysis provides a valuable information to identify such regions. Our results indicate that global whipping is not expected for low and moderate applied pressure drops and liquid viscosities. In this case, the nozzle configuration might be recommendable.

Important biomedical and biotechnological applications ranging from cell microencapsulation to sorting are impacted by the smooth and gentle nature of the flow stream, the clean device shape and the minimization of the amount of effluents (focusing fluids) in flow focusing with nozzles. In this regard, this technique offers considerable advantages over any other alternative method, significantly reducing costs associated with operational safety, compactness, handling, inspection and cleaning. The smoothness of the nozzle orifice and its smaller size reduce the inherent noise associated with the turbulence in the expelled gas stream as compared with the standard plate-orifice counterpart.

Acknowledgments

Partial support from the Ministry of Science and Education, Junta de Extremadura, and Junta de Andalucía (Spain) through grants nos DPI2010-21103, GR10047 and P08-TEP-04128, respectively, is gratefully acknowledged.

References

[1] Eggers J 1997 Nonlinear dynamics and breakup of free-surface flows *Rev. Mod. Phys.* **69** 865–929
[2] Eggers J and Villermaux E 2008 Physics of liquid jets *Rep. Prog. Phys.* **71** 1–79
[3] Basaran O A 2002 Small-scale free surface flows with breakup: drop formation and emerging applications *AlChE J.* **48** 1842–8
[4] Eggers J and du Pont S C 2009 Numerical analysis of tips in viscous flow *Phys. Rev.* E **79** 066311
[5] Blanchette F and Zhang W W 2009 Force balance at the transition from selective withdrawal to viscous entrainment *Phys. Rev. Lett.* **102** 144501
[6] Guillot P, Colin A, Utada A S and Ajdari A 2007 Stability of a jet in confined pressure-driven biphasic flows at low Reynolds numbers *Phys. Rev. Lett.* **99** 104502
[7] Gañán-Calvo A M 1998 Generation of steady liquid microthreads and micron-sized monodisperse sprays in gas streams *Phys. Rev. Lett.* **80** 285–8
[8] Gañán-Calvo A M, González-Prieto R, Riesco-Chueca P, Herrada M A and Flores-Mosquera M 2007 Focusing capillary jets close to the continuum limit *Nature Phys.* **3** 737–42
[9] Gañán-Calvo A M, Pérez-Saborid M, López-Herrera J M and Gordillo J M 2004 Steady high viscosity liquid micro-jet production and fiber spinning using co-flowing gas conformation *Eur. Phys. J.* B **39** 131–7
[10] Anna S L, Bontoux N and Stone H A 2003 Formation of dispersions using flow focusing in microchannels *Appl. Phys. Lett.* **82** 364–6
[11] Dollet B, van Hoeve W, Raven J-P, Marmottant P and Versluis M 2008 Role of the channel geometry on the bubble pinch-off in flow-focusing devices *Phys. Rev. Lett.* **100** 034504
[12] Si T, Li F, Yin X-Y and Yin X-Z 2009 Modes in flow focusing and instability of coaxial liquid-gas jets *J. Fluid Mech.* **629** 1–23
[13] Gañán-Calvo A M and Montanero J M 2009 Revision of capillary cone-jet physics: electrospray and flow focusing *Phys. Rev.* E **79** 066305

[14] Vega E J, Montanero J M, Herrada M A and Gañán-Calvo A M 2010 Global and local instability of flow focusing: the influence of the geometry *Phys. Fluids* **22** 064105
[15] Montanero J M, N. Rebollo-Muñoz, Herrada M A and Gañán-Calvo A M 2011 Global stability of the focusing effect of fluid jet flows *Phys. Rev.* E **82** 036309
[16] Lin S P and Lian Z W 1989 Absolute instability of a liquid jet in a gas *Phys. Fluids* A **1** 490–3
[17] Huerre P and Monkewitz P A 1990 Local and global instabilites in spatially developing flows *Annu. Rev. Fluid Mech.* **22** 473–537
[18] Gañán-Calvo A M, Ferrera C and Montanero J M 2011 Universal size and shape of viscous capillary jets: application to gas-focused microjets *J. Fluid Mech.* **670** 427–38
[19] Clarke N S 1966 A differential equation in fluid mechanics *Mathematika* **12** 51–3
[20] Clarke N S 1968 Two-dimensional flow under gravity in a jet of viscous liquid *J. Fluid Mech.* **31** 481–500
[21] DePonte D P, Weierstall U, Schmidt K, Warner J, Starodub D, Spence J C H and Doak R B 2008 Gas dynamic virtual nozzle for generation of microscopic droplet streams *J. Phys. D: Appl. Phys.* **41** 1–7
[22] Montanero J M, Gañán-Calvo A M, Acero A J and Vega E J 2010 Micrometer glass nozzles for flow focusing *J. Micromech. Microeng.* **20** 075035
[23] Chapman H N *et al* 2011 Femtosecond x-ray protein nanocrystallography *Nature* **470** 73–9
[24] Morse P M and Feshbach H 1953 *Methods of Theoretical Physics* (New York: McGraw-Hill)
[25] Cabezas M G, Bateni A, Montanero J M and Neumann A W 2005 A new method of image processing in the analysis of axisymmetric drop shapes *Colloids Surf.* A **255** 193–200
[26] Tang K and Gómez A 1996 Monodisperse electrosprays of low electric conductivity liquids in the cone-jet mode *J. Colloid Interface Sci.* **184** 500–11
[27] Zhmayev E, Zhou H and Joo Y L 2008 Modeling of non-isothermal polymer jets in melt electrospinning *J. Non-Newtonian Fluid Mech.* **153** 95–108
[28] Lasheras J C and Hopfinger E J 2000 Liquid jet instability and atomization in a coaxial gas stream *Annu. Rev. Fluid Mech.* **32** 275–308
[29] Tammisola O, Lundell F and Soderberg L D 2011 Effect of surface tension on global modes of confined wake flows *Phys. Fluids* **23** 014108
[30] Tritton D J 1988 *Physical Fluid Dynamics* (Oxford: Oxford University Press)
[31] Entov V M and Yarin A L 1984 The dynamics of thin liquid jets in air *J . Fluid Mech.* **140** 91–111
[32] Herrada M A, Ferrera C, Montanero J M and Gañán-Calvo A M 2010 Absolute lateral instability in capillary coflowing jets *Phys. Fluids* **22** 064104
[33] Juniper M P and Candel S M 2003 The stability of ducted compound flows and consequences for the geometry of coaxial injectors *J. Fluid Mech.* **482** 257–69
[34] Rees S J and Juniper M P 2009 The effect of surface tension on the stability of unconfined and confined planar jets and wakes *J. Fluid Mech.* **633** 71–97
[35] Leib S J and Goldstein M E 1986 Convective and absolute instability of a viscous liquid jet *Phys. Fluids* **29** 952–4